USING ARTIFICIAL NEURAL NETWORK TO PREDICT THE FRACTURE PROPERTIES OF THE INTERFACIAL TRANSITION ZONE OF CONCRETE AT THE MESOSCALE

Xun Xi[1], Ziqing Yin[1], Shangtong Yang[1,2*], Chun-Qing Li[3]

[1]*Department of Civil and Environmental Engineering, University of Strathclyde, Glasgow G1 1XJ, United Kingdom.*

[2]*Key Laboratory of Performance Evolution and Control for Engineering Structures (Tongji University), Ministry of Education, China.*

[3]*School of Engineering, RMIT University, Melbourne, Vic 3001, Australia.*

Abstract

Concrete is a multi-phase heterogeneous material in which the interfacial transition zone (ITZ) between aggregates and mortar significantly affects the cracking behaviour of concrete, especially under tensile load. In this paper, the artificial neural network (ANN) method is applied in predicting the fracture properties of ITZ in concrete. To form the data pool for the training of the ANN, a large number of two-dimensional (2D) meso-scale fracture simulation of concrete under direct tensile load is conducted. Cohesive crack elements are used in simulating arbitrary cracking in the ITZ and mortar. After the verification of the trained ANN model, the tensile strength and fracture energy of the concrete ITZ are predicted by using the RILEM direct tensile test results, i.e., stress–displacement curve, as the input for the ANN. It has been found that, the trained ANN performs well in predicting the ITZ properties and the computed stress–displacement curve together with the optimized ITZ fracture parameters has a good agreement with that from the RILEM test results. The randomness of aggregates has little effect on the predicted ITZ tensile strength while it becomes slightly bigger on the predicted ITZ fracture energy. The tensile strength ratio of ITZ to mortar are calculated 0.38-0.47 and the fracture energy ratio of ITZ to mortar are 0.18-0.58. These inversely predicted fracture properties of concrete ITZ can be useful complementation to the existing dataset and 2D fracture simulation of concrete structures.

Keywords: interfacial transition zone (ITZ); cohesive elements; fracture energy; inverse analysis; artificial neural network.

* Corresponding author. Tel: +44 141 548 3273. Email: shangtong.yang@strath.ac.uk.

1. Introduction

As the most widely used construction material worldwide, concrete has attracted considerable research interest in the past few decades particularly for improved sustainability, enhanced strength and prolonged service life. To better understand the concrete properties and develop new concretes [1-4] to satisfy the pressing demands from the changing environment, the meso-scale structure of concrete and their relationship with the exhibited engineering properties becomes a key. At the meso-scale, concrete is made of multi-phase material components and the interfacial transition zone (ITZ) between the aggregates and the (mortar) matrix is normally the weakest part in such a composite [5-7]. Therefore, the mechanical behaviour, especially the fracture properties, of the ITZ in concrete in important in predicting the concrete performance.

The size of fracture process zone (FPZ) during concrete cracking is not small enough for negligible so concrete is normally considered as a quasi-brittle material. Hillerborg et al. [8] proposed the cohesive crack model to characterize the behaviour of a finite-size FPZ, which has developed to become one of the most robust fracture models for concrete. There are two independent parameters in the cohesive law: the tensile strength and fracture energy. So far, lots of researches have been carried out to measure the strength and fracture energy of concrete by experiments [9, 10]. In particular, several methods including three-point bending test [11], compact tension test [12], wedge splitting test [13] and uniaxial tensile test [14], have been proposed to determine the strength and fracture energy for concrete. Amongst the proposed methods, the uniaxial tensile test is the direct and most accurate method for obtaining the stress–displacement (of notch) relation which represents the true uniaxial mechanical behaviour compared to others [9]. However, it should also be mentioned that, most experimental and theoretical work were focused on Mode I fracture while studies on Mode II fracture properties have not been very clearly understood yet. It is even questionable that Mode

II fracture energy obtained from the test is the real material property [15]. The argument is related to the fact that creating a pure Mode II fracture for quasi-brittle materials in experiment is extremely challenging [10].

Compared with other the aggregates and cement mortar, the fracture properties of ITZ are much more difficult to be tested. Rao and Prasad [16] designed notched rock-mortar specimens by casting fresh mortar on the rock surface and found that the tensile strength of interface between the rock and mortar was 1/16 – 1/3.5 times of that of mortar. Gu et al. [17, 18] tested the bonding strength of the ITZ and found the bonding strength was about 50% of the tensile strength of the mortar. Dong et al. [19] carried out the three-point bending test for a concrete-rock beam with the interface located at the geometric centre; they obtained the tensile strength and fracture energy of ITZ which were 1.37 MPa and 19.3 N/m, respectively. Meanwhile, the ITZ properties are closely related to the processing and manufacturing of concrete including mixing, transportation, compaction, etc. Moreover, by nano-indentation test, Xiao et al. [5] obtained the elastic modulus and hardness of ITZ in concrete and found that the hardness value for ITZ were about 80% - 85% of that for mortar. However, it should also be noted that the nano-indentation results on ITZ properties are at different length scale to above mentioned meso-scale ITZ tests and they may not be directly comparable.

In the past decade, some researchers proposed to model concrete arbitrary cracking by inserting zero-thickness cohesive elements into the mesh of multi-phase concrete [6, 7, 20-26]. The meso-scale modelling based on cohesive elements provides an effective approach to investigate the toughening fracture mechanism of concrete cracking, such as aggregate bridging, void formation, or microcrack shielding. Yang et al. [6, 21, 22] modelled concrete fracture under the uniaxial tensile test in 2D as a heterogeneous material by inserting cohesive elements and

the heterogeneity was achieved by random aggregates distribution [6, 22] or random elements properties [21]. Further, Ren et al. [7] obtained more realistic concrete meso-structures through X-ray computed tomography scanning and carried out 2D uniaxial tensile simulations by the imaged based mesh with cohesive elements. They found that the micro cracks were always initiated at the ITZ before connected to form the macro cracks and the overall stress-displacement relationship of concrete was mainly determined by ITZ fracture properties. Recently, Ren et al. [27] and Trawiński et al. [26] established 3D numerical model using cohesive elements based on X-CT scanning results of concrete specimen and modelled the concrete cracking under direct uniaxial loading. Their researches revealed that 3D modelling would be a very powerful tool to unveil the damage and failure mechanisms in a more realistic way. However, 3D simulations for concrete fracture at meso-scale level, due to the highly nonlinear equation system and the softening-induced instabilities, are very time-consuming [26]. The limitation on computing efficiency brings great challenges in the widespread application of 3D meso-scale fracture models especially when a large number of simulations are necessary.

Trial and error is usually used to estimate the ITZ properties for application in the meso-scale simulation of concrete cracking. However, this method cannot always yield accurate and reliable results. Instead, inverse analysis method has been widely employed to determine the mechanical parameters of materials and structures, such as rock creep parameter [28], residual stress by wilding [29] and overall fracture properties of composites [28, 30, 31]. Recently the application of artificial intelligence in civil engineering has proved powerful and has potential to solve new problems. In light of the fracture properties of the concrete ITZ, given the difficulties in the experimentation, an inverse method based on artificial neural network would be a promising solution.

This paper aims to use the artificial neural network (ANN) in the prediction of the fracture properties of ITZ in concrete. Concrete is considered as a heterogeneous material at the meso-scale, consisting of polygonal aggregates, mortar and ITZ. A multi-phase fracture model involving cohesive elements is established and the uniaxial direct tensile test from RILEM is employed and reproduced in the finite element simulation. A large number of simulations are conducted with prior known values of ITZ tensile strength and fracture energy to form the data pool to train the ANN. After the training and validation of the ANN, the real ITZ tensile strength and fracture energy are inversely attained, against the RILEM test results. A parametric study focusing on some underlying factors that may influence the accuracy of the ANN prediction on the fracture properties of ITZ in concrete is carried out.

2. Meso-scale fracture model for concrete

A meso-scale structure for concrete is firstly developed by randomly generating and packing aggregates. Although realistically aggregates should have rough edges, it is almost impossible to mesh the aggregates with extremely irregular edges in finite element modelling [7, 17]. We simplified the aggregate shape as the polygon with a random size and 4 to 13 sides. An aggregate in a regular polygon (Figure 1a) is generated with random sides in 4 - 13 and a random size in a specified grading range. To change the regular polygon to irregular one, the vertex of the regular polygon will be randomly moved to/away from the centre and then rotated between the adjacent vertices (Figure 1b and 1c).

Once the meso-structure of concrete is generated and meshed, cohesive elements are embedded into the boundaries of the mesh. The ITZ and mortar matrix have cohesive elements inserted to approximately simulate arbitrary cracking but the material properties of the cohesive

130 elements are defined separately for these two phases. The mechanical properties of aggregates
131 are considerably stronger than mortar and the ITZ excluding the ultra-high performance
132 concrete (UHPC). In this study, the fracture of aggregates is not simulated and the ITZ is
133 assumed as zero thickness interface. More details on the insertion process of cohesive elements
134 has been introduced in the authors' previous study [32]. Figure 2 shows the concrete model
135 consisting of solid elements for the aggregates and mortar, and cohesive elements in the mortar
136 and the interfaces. The mesh size is 1 mm for the worked example and we will discuss the mesh
137 dependency later.
138
139 Normally, a traction–separation law is used as the constitutive model for the zero-thickness
140 cohesive elements [7]. The calculation thickness for the cohesive elements is 1 so the element
141 strain is replaced by the relatively displacement of the crack face. The traction stress of
142 cohesive elements is a function of the corresponding relative displacements of the crack surface.
143 In general, the traction–separation laws for the cracks can be expressed as follows:

144 $$\sigma_n = f(\delta_n) \tag{1}$$

145 $$\sigma_s = f(\delta_s) \tag{2}$$

146 where σ_n and σ_s are the normal and shear traction stress, respectively. δ_n and δ_s are the
147 corresponding opening displacement and slipping displacement, respectively; f is the function
148 describing the traction and separation relationship.
149
150 For a cohesive crack, the traction stresses will linearly increase to the peak strength by a penalty
151 stiffness and then gradually decrease to zero. The traction–separation relationship for the
152 opening and shearing in the linearly elasticity stage can be expressed as follows:

153 $$\sigma_n = K_n < \delta_n > \tag{3}$$

154 $$\sigma_s = K_s \delta_s \tag{4}$$

where < > is the Macaulay bracket which equals zero if the value of normal displacement is smaller than zero (i.e., compression). The K_n and K_s are the penalty stiffness at the normal and shear directions, respectively. Penalty stiffness is a numerical parameter to control the deformation of the zero-thickness cohesive element.

Figure 3 illustrates the constitutive relationship for the cohesive crack with an exponential post-peak softening behaviour. The area under the traction-separation curve is the corresponding fracture energy. It should be mentioned that, the softening behaviour can be in a linear, bilinear even any pre-defined shape. The damage initiation will occur when the critical displacement satisfies the following equation:

$$\left(\frac{\sigma_n}{\sigma_n^0}\right)^2 + \left(\frac{\sigma_s}{\sigma_s^0}\right)^2 = 1 \quad (5)$$

where σ_n^0 and σ_s^0 are the tensile strength and shear strength of the cohesive crack, respectively. It should be mentioned that the experimental data on the shear fracture properties are very limited [7]. Although some researches considered the shear strength was larger than tensile strength and proposed to use the ratio of shear strength to tensile strength to model concrete cracking, the ratio was randomly assumed and not verified by experiments [20, 34]. Moreover, there is even a doubt whether shear fracture energy is a material property [15, 20]. For uniaxial direct tensile test, tensile fracture is the main failure type. As such, Mode I fracture properties are considered as most significant parameters in the simulations and the parameters for Mode II fracture are assumed to be the same as those for Mode I fracture according to existing studies on tensile fracture modelling of meso-scale concrete [21, 24, 26, 35].

An effective displacement coupling normal and shear separation is proposed to calculate the damage evolution:

$$\delta = \sqrt{< \delta_n >^2 + (\delta_s)^2} \quad (6)$$

where δ is the effective displacement.

Further, the damage value under the exponential damage curve can be calculated as follows [24]:

$$D = 1 - (\frac{\delta_0}{\delta_m})\left\{1 - \frac{1-\exp\,(-\alpha(\frac{\delta_m-\delta_0}{\delta_f-\delta_0}))}{1-\exp\,(-\alpha)}\right\} \quad (7)$$

where δ_0 is the critical displacement when the stress reaches the peak strength (i.e., D=0); Due to the same value of tensile and shear strength, the critical displacements for the pure tensile, pure shear and mixed-mode cracking become the same (the inner circle in Figure 3). δ_m is the maximum effective displacement during the loading history; δ_f is the completely failure displacement which is the same for the pure tensile, pure shear and mixed-mode cracking (i.e., the outer circle in Figure 3). α is a softening parameter representing the damage evolution rate.

Thus, the post-peak traction stresses can be expressed as follows:

$$\sigma_n = (1 - D)K_n < \delta_n > \quad (8)$$

$$\sigma_s = (1 - \mathrm{D})K_s\delta_s \quad (9)$$

It should be mentioned that, D is the stiffness damage value while not the strength damage value. Once the cohesive strength σ_0, failure displacement δ_f and the softening parameter α are determined, the fracture energy (i.e., the area under the softening curve) can be obtained as follows:

$$G_f = \int_0^{\delta_f} f(\delta)\,\delta \quad (10)$$

For quasi-static simulations by implicit analysis programs, a small value of viscosity can be introduced to help convergence, making the stiffness matrix positive definite. The viscosity

regularizes the constitutive relationship of the cohesive element by modifying the damage value D to D_v as follows:

$$\dot{D_v} = (D - D_v)/\mu \tag{11}$$

where D_v is the viscous damage variable for regularization of the constitutive equations. $\dot{D_v}$ is the derivative of viscous stiffness degradation variable with respect to time; μ is the viscosity parameter which should be sufficiently small to improve the rate of convergence without compromising results. When viscosity is introduced to the model, D is not applicable any more while D_v becomes effective. The material stiffness matrix is then modified.

3. Direct tensile test on fracture properties of concrete

RILEM [11, 14] recommended a closed-loop uniaxial tensile test method to obtain the stress–displacement relationship which describes the overall fracture behaviour for concrete. The experimental data on RILEM round-robin tests [11, 14] is used to validate the developed numerical method and the starting point for the inverse analysis. In the round-robin tests, the mix proportion by weight for concrete was 1:2:2.5:0.56 in terms of cement, fine aggregate, coarse aggregate and water respectively. In addition, 10 mm single-sized coarse aggregates were used. The coarse aggregates were defined as aggregates with size larger than 2.36 mm according to British Standard 882 [36]. To reduce the complexity of the mesh, only coarse aggregates larger than 2.36 mm are modelled in this study, while fine aggregates and cement are treated as mortar phase [22]. The total area fraction of coarse aggregates can be calculated by the weight mix proportion and materials densities as follows:

$$P_a = \frac{P_w/\rho_{agg}}{\rho_{con}} \tag{12}$$

where P_a is the area/mass percentage of the coarse aggregates in the total. P_w is the percentage by weight of the coarse aggregates in the total, which is about 0.41 according to the mix

proportion by weight in their experiments [11, 14]. ρ_{agg} and ρ_{con} are the density of the coarse aggregate (limestone) and the normal concrete, respectively. The values of density for limestone and normal concrete are about 2400 kg/m^3 and 2700 kg/m^3, respectively [37]. The calculated area fraction of the coarse aggregates is about 36.7% by Equation (12). More details on the experiments can be found in the references [11, 14].

A 2D concrete model with the same size of the experimental sample is developed. The model dimensions are 100 mm×150 mm and two notches are created with width 2 mm and depth 10 mm in the middle of the model. Figure 2 shows the typical mesh with element size 1 mm. Table 2 lists the values for the geometric and mechanical parameters and their sources. Yang et al. [7] have found that the interfacial cohesive strength and fracture energy are the dominant factors governing the fracture process of concrete. Rao et al. [38] investigated the relationship between the mortar splitting tensile strength and the water/cement ratio and generalized the Abrams' law for predicting the tensile strength of mortar. In Rao's experiments, the mortar tensile strength changes from 1.76 to 2.66 MPa when the water/cement ratio decreases from 0.65 to 0.3. According to Abrams' generalization law, the mortar strength for the water/cement ratio 0.56 was estimated as 2.2 MPa [38]. Further, the fracture energy of the mortar was predicted as 72N/m according to Rao's experimental data on mortar fracture energy [16]. Moreover, a parametric study of a realistic range of tensile strength and fracture energy of mortar on the fracture behaviour of the concrete sample in this research will be carried out. The damage evolution rate parameter α is obtained by fitting the Equations (7) and (8) with RILEM data [11, 14]. The tensile strength and fracture energy of ITZ are regarded as targets which will be inversely determined. The effects of mortar strength and fracture energy on the inverse analysis will be investigated by parametric studies later.

252 The top and bottom surfaces of the specimen for experiments were tied to the loading plates
253 by stiff glue [11]. For the direct uniaxial tension modelling, the frictional and rotational effects
254 were considered minor and the tensile displacements (y direction) were directly applied to top
255 and bottom nodes. The average stress of the model is obtained by dividing the reaction forces
256 by the net cross section area. The crack width w is obtained from the average value of the
257 separating displacements of the two notches.
258
259 **4. Establishing the artificial neural network and the inverse analysis**
260 The artificial neural network (ANN) has been widely employed for learning, predictions and
261 making decisions based on data. There are three basic datasets for the ANN model: training,
262 testing and validation datasets. First, training dataset is used to fit the model. Then testing
263 dataset is used to provide an unbiased evaluation of a final model fit on the training dataset.
264 The validation is to evaluate a given model by a dataset [39]. The inverse analysis method
265 based on ANN for determining the ITZ fracture properties of concrete is as follows: First, a
266 known solution for the overall fracture behaviour (i.e., the whole stress-crack width
267 relationship) should be obtained with a high reliability and accuracy. Then, a meso-scale
268 concrete model consisting of aggregates, mortar and ITZ should be developed. This model is
269 able to obtain the overall structural performance and the whole stress-crack width curve of the
270 concrete by assigning different material properties to different phrases. We select the tensile
271 strength and fracture energy of ITZ as the target variables and the other material parameters
272 are treated as constants. Numerical simulations with a number of initial values for the tensile
273 strength and fracture properties of ITZ are conducted. Accordingly, the stress-crack width
274 curves from the simulations can be obtained. For establish the ANN, the initial values for the
275 tensile strength and fracture energy of ITZ are used as input data and the stress-crack width
276 curves from the corresponding simulations are output data. These input and output data are

277 randomly divided into training, testing and validation dataset. Then an objective function for
278 calculating the error between the computed outputs and experimental stress-crack width curve
279 is created in the ANN. For a given output value (i.e., the overall stress-crack width curve), an
280 optimization algorithm is used to find optimized ITZ values which make the objective function
281 minimum. Further, the computed stress-crack width curve with optimized values will be
282 compared with experimental results. Then, the error between the numerical and experimental
283 results are calculated. If the error falls below a threshold value, i.e., negligibly small, the ITZ
284 values are determined and the inverse analysis processes are accomplished. If the error is over
285 the threshold value, the current numerical results will be added to re-train the network and
286 inverse the targeted ITZ fracture properties. However, it is likely that the errors cannot be
287 reduced even after lots of iterations. In this case, the retraining and inverse analysis will be
288 forced to quit and the ITZ properties will be determined by the final inverse analysis with the
289 corresponding error. The maximum iterations for retraining is set as 10 in this study.
290
291 RILEM uniaxial direct tensile test [14] obtained the whole stress-crack width curve of concrete
292 which is chosen as the known solution. The developed meso-scale fracture model for concrete
293 is used to generate the input and output data for establishing the ANN. The uniform design
294 which uniformly scatters the design points in the domain range is employed for choosing the
295 initial values for the ITZ tensile strength and failure displacement. Figure 4 illustrates the 20
296 sets of input values for ITZ fracture properties according to the previous studies on ITZ
297 properties [5, 16-19]. The initial ITZ values and their corresponding stress-crack width curves
298 from simulations are then used as the ANN training, testing and validation input and output
299 data, respectively. The ANN is established in Matlab and the output for the stress-crack width
300 curve is read by a Matlab open-source application [40]. It should be mentioned that, the stress-
301 crack width curves from simulations and experiments are represented by 40 discrete points

302 which are linearly spaced to train the ANN. Figure 5 shows the computed stress-crack width
303 curves. An objective function considering both the errors of peak point and all the 40 points at
304 the stress-crack width curve is designed as follows:

305 $$\text{Fit} = \min \sum_{i=1}^{40} \left\{ \frac{[\max(y_i) - \max(x_i)]^2}{[\max(x_i))]^2} + \frac{(y_i - x_i)^2}{[\text{sum}(x_i))]^2} \right\} \quad (13)$$

306 where y_i and x_i are the stresses for the i^{th} point from the network and the experiment,
307 respectively; The max(y_i) and max(x_i) are the maximum stresses (i.e., tensile strength) from the
308 network and the experiment, respectively.
309
310 Back-propagation (BP) algorithm is used to train the network. In this method, the error
311 calculated at the output of the network is propagated back through the layers of neurons to
312 update the weights [39]. The network contains 8 hidden layers and the account for training,
313 validation and testing dataset 80%, 10% and 10%, respectively. Figure 6(a)-(d) show the linear
314 regression of network outputs with respect to targets for training, validation, testing and all sets.
315 The targets are the values of simulated stress at the 40 points from simulations while the outputs
316 are the values of stress at the 40 points predicted from the network. The *R* values for all the
317 datasets are larger than 0.99, which means the fit is very good and the output tracks the targets
318 very well for all datasets. Figure 7 shows the variations of Mean Squared Error of the outputs
319 for the learning and testing sets plotted against different number of epochs. The error quickly
320 decreases to smaller than 0.001 with epochs increasing and the errors of testing and validation
321 sets have similar characteristics. Moreover, overfitting does not occur because neither testing
322 nor validation error increased before epoch 32. Therefore, the established ANN can well predict
323 the target variables.
324
325 The optimized tensile strength and fracture energy for concrete ITZ are 1.02 MPa and 28.9
326 N/m, respectively. Figure 8 shows the stress-crack width curves from both the numerical model

with the optimized ITZ fracture properties and the RILEM experiment [14]. The computed stress-crack width curve has a good agreement with that from RILEM experiment. The error between the two curves by Equation (13) is 1.8%. Therefore, the ITZ tensile strength and fracture energy can be well predicted by the ANN. The ratio of ITZ tensile strength to mortar tensile strength is about 0.46 time and the fracture energy of ITZ is about 0.4 time of the fracture energy of the mortar.

5. Parametric study and discussion

The aggregates in the heterogeneous concrete model are randomly generated and packed. Therefore, the heterogeneity of concrete will affect the concrete cracking. Figure 9 illustrates the effect of concrete heterogeneity on the stress-displacement curves by 10 random heterogeneous models which use the same materials mechanical parameters including the optimized ITZ fracture properties. It can be seen that, the stress-displacement curves are very close at the linear increase stage before the peak-stress and have slight differences at the softening stage. Although the stress-displacement curve has a reasonable repeatability, the variabilities may affect the values of optimized ITZ fracture properties. Further, based on the same 20 sets of initial values for simulations and the inverse method, the ITZ fracture properties for each heterogeneous model are determined. Table 2 shows the values of the optimized ITZ tensile strength, fracture energy, iteration number and error. It can be found that, the tensile strength varies from 0.96-1.03 MPa and the fracture energy varies from 13.1-28.9 N/m for different heterogeneous models. Figure 10 illustrates the stress-displacement curves from RILEM experiment and the numerical simulations with optimized ITZ fracture properties. The error between the stress-displacement curves from the experiment and numerical simulation varies from 0.6% to 3.1%, which proves the numerical model and inverse analysis method are reliable. The mean value and coefficient of variation for the ITZ tensile strength are 1.00 MPa

352 and 2.8%, respectively. Therefore, the determined ITZ tensile strength is about 0.46 time of
353 the mortar strength. The mean value and coefficient of variation for the fracture energy of ITZ
354 are 20.9 N/m and 27%, respectively. The ratio of the ITZ fracture energy to mortar fracture
355 energy is about 0.18-0.40 with a relatively high degree of variability. The values obtained for
356 ITZ will be useful in the meso-scale modelling of concrete fracture; however, it may be noted
357 that more cases should be included in the inverse analysis by considering a variety of material
358 composition and geometric configuration. It will then give a range of values for ITZ properties
359 and the possible correlation to some underlying parameters. Figure 11 shows the typical crack
360 patterns for three heterogeneous models. It can be found that, the macro cracks are formed at
361 the middle of the specimen and the interfaces dominate the crack path. It is interesting to find
362 that, two macro cracks occur for model 9 where the cracks propagate from two notches. Due
363 to the distributions of aggregates and driving effects of ITZ, the left crack propagates to the top
364 of the right notch. Although the post-peak stress has decreased to about zero, the two macro
365 cracks have not completely connected.

366

367 As introduced in Equation (11), the viscosity is a numerical parameter to overcome the
368 convergence problem. Parametric studies are carried out to investigate the effect of viscosity
369 on the stress-displacement curve and crack pattern. Figure 12 illustrates the stress-displacement
370 curves for the heterogeneous model 1 with the viscosity values 1.0×10^{-5}, 5.0×10^{-5} and 1.0×10^{-4}. It can be seen that, the smaller the viscosity is, the smaller the peak strength of concrete is.
372 A very small value of viscosity has little effect on the stress-displacement curve. However, the
373 increment steps for the simulations with the viscosity values 1.0×10^{-5}, 5.0×10^{-5} and 1.0×10^{-4}
374 are 1640, 624 and 432, respectively. The convergence can be significantly improved by a
375 relatively larger viscosity. Figure 13 shows the crack patterns of the heterogeneous model 1 for
376 different values of viscosity. It can be seen that, there is no difference in the crack patterns of

heterogeneous model 1 with the viscosity 1.0×10^{-5}, 5.0×10^{-5} and 1.0×10^{-4}. Therefore, the viscosity in this study is determined as 5.0×10^{-5} for improving the convergence without compromising results.

Although the mesh dependency has been reduced through replacing the strain by separation displacement in the constitutive model of cohesive element, the crack patterns and overall stress-displacement may also be mesh-dependent if the size ratio of fracture process zone to cohesive element is not large enough. Figure 14 illustrates the stress-displacement curves for the heterogeneous model 1 with element size 0.5 mm, 1 mm and 2 mm. It can be found that, the stress-displacement curves are almost the same for the meshes with the three chosen element sizes. The increment steps for the simulations with element size 0.5 mm, 1 mm and 2 mm are 3079, 624 and 764, respectively. Figure 15 shows the crack patterns for the heterogeneous model 1 with the three element sizes. It can be seen that, the element size has little effects on the crack patterns while the crack paths are slightly different for the three element sizes. In consideration of calculation efficiency, the smaller the element size is, the larger the degree of freedom of the mesh is and more CPUs time will be required for each increment step. Therefore, the element size is set as 1 mm in this study.

It has been found that the ITZ fracture properties dominate the overall fracture of concrete for uniaxial tensile tests [23, 27, 42]. However, it should be mentioned that the tensile strength and fracture energy of the mortar in this study are estimated according to previous experiments [16, 38]. Therefore, the effects of mortar tensile strength and fracture energy on the inversed results are investigated. The optimized values of tensile strength and fracture energy from the inverse analysis of heterogeneous model 8 are listed in Table 3. It can be seen that, for the mortar tensile strength varying from 1.9 to 2.5 MPa, the optimized ITZ tensile strength and fracture

energy change from 1.10-0.94 MPa and 31.9-22.5 N/m, respectively. The larger the mortar strength is, the smaller the optimized ITZ tensile strength and fracture energy are. The mean values of the optimized ITZ tensile strength and fracture energy are 1.05 MPa and 29.6 N/m, respectively. In addition, the values for coefficient of variation of the optimized ITZ tensile strength and fracture energy are 7.1% and 15.8%, respectively. Figure 16 shows the stress-displacement curves from the inversed results with different mortar strengths and fracture energies. It can be found that, the stress-displacement curves from the simulations have a good agreement with that from experimental results. Figure 17 illustrates the crack pattern for the heterogeneous model 8 with different mortar strengths and fracture energies. It can be seen that, the crack patterns from the inversed results are almost the same.

6. Conclusions

This paper proposed a method to inversely determine the ITZ fracture properties of concrete based on meso-scale concrete fracture model and artificial neural network. A three-phase concrete model containing aggregate, mortar and ITZ was developed and zero-thickness cohesive elements were used to simulate the cracking in the mortar and ITZ. RILEM direct uniaxial tensile test was employed as the worked example to demonstrate the inverse method and the benchmark to inversely determine the ITZ properties. A number of simulations with initial ITZ fracture properties were carried out to obtain the stress-displacement curves which was used for training the artificial neutral network. Various factors have been considered in the parametric study in confirming the robustness of the developed method. Specific conclusions can be obtained as follows:

(1) The developed fracture model can reproduce the cracking phenomena (i.e., micro cracks initiation, crack deflection, bridging etc.) of concrete at meso-scale. The

established artificial neural network showed a good performance in optimizing the fracture properties of ITZ by minimizing the objective function. The computed stress-crack width curve with the optimized tensile strength and fracture energy of ITZ has a good agreement with that from the RILEM experiment. The proposed method is robust and reliable on determining the tensile strength and fracture energy of ITZ once the mortar and aggregate properties are obtained.

(2) For 10 different heterogeneous models, the mean values and coefficients of variance for ITZ tensile strength and fracture energy are 1.0 MPa and 2.8%, 20.9 N/m and 27%, respectively. The randomness of aggregates has little effect on the optimized ITZ tensile strength but slightly bigger effect on the optimized ITZ fracture energy.

(3) The larger the tensile strength of mortar is, the smaller the optimized ITZ strength and fracture energy are. However, in the ranges of mortar strength (1.9-2.5 MPa) and fracture energy (60-92 N/m), the values for coefficient of variation of the optimized ITZ tensile strength and fracture energy are 7.1% and 15.8%, respectively. The optimized ITZ results would be reliable according to the estimations of mortar fracture properties.

(4) The tensile strength ratio of ITZ to mortar are 0.38-0.47 and the fracture energy ratio of ITZ to mortar are 0.18-0.58 according to the parametric study on aggregate randomness and variety of mortar fracture properties. These ratios can well be used for meso-scale fracture modelling of concrete. It should be noted, however, that these values were derived without the consideration of more complex 3D mechanisms including aggregate distribution and the heterogeneity out of the plane. Therefore, the accuracy of directly using these data in 3D meso-scale fracture simulation of concrete is not verified.

Acknowledgements

This project was supported by Key Laboratory of Performance Evolution and Control for Engineering Structures (Tongji University), Ministry of Education (No. 2019KF-1), China. Moreover, simulations were performed using ARCHIE-West High Performance Computer based at the University of Strathclyde, UK. They are both gratefully acknowledged.

References

[1] D. Fukuda, Y. Nara, Y. Kobayashi, M. Maruyama, M. Koketsu, D. Hayashi, H. Ogawa, K. Kaneko, Investigation of self-sealing in high-strength and ultra-low-permeability concrete in water using micro-focus X-ray CT, Cem. Concr. Res. 42(11) (2012) 1494-1500.
[2] D. Fan, S. Yang, Mechanical properties of C-S-H globules and interfaces by molecular dynamics simulation, Constr. Build. Mater. 176 (2018) 573-582.
[3] M.B. Leite, P.J.M. Monteiro, Microstructural analysis of recycled concrete using X-ray microtomography, Cem. Concr. Res. 81 (2016) 38-48.
[4] H. Zhang, Y.J. Huang, Z.J. Yang, S.L. Xu, X.W. Chen, A discrete-continuum coupled finite element modelling approach for fibre reinforced concrete, Cem. Concr. Res. 106 (2018) 130-143.
[5] J. Xiao, W. Li, D.J. Corr, S.P. Shah, Effects of interfacial transition zones on the stress–strain behavior of modeled recycled aggregate concrete, Cem. Concr. Res. 52 (2013) 82-99.
[6] X. Wang, M. Zhang, A.P. Jivkov, Computational technology for analysis of 3D meso-structure effects on damage and failure of concrete, Int. J. Solids. Struct. 80 (2016) 310-333.
[7] W. Ren, Z. Yang, R. Sharma, C. Zhang, P.J. Withers, Two-dimensional X-ray CT image based meso-scale fracture modelling of concrete, Eng. Fract. Mech. 133 (2015) 24-39.
[8] A. Hillerborg, M. Modeer, P.E. Petersson, Analysis of crack formation and crack growth in concrete by means of fracture mechanics and finite elements, Cem. Concr. Res. 6(6) (1976) 773-781.
[9] S. Khalilpour, E. BaniAsad, M. Dehestani, A review on concrete fracture energy and effective parameters, Cem. Concr. Res. 120 (2019) 294-321.
[10] Q. Lin, S. Wang, P.Z. Pan, W.W. Ji, Y. Lu, Fracture initiation under pure shear revisited: Remarks on the mode II fracture in quasi-brittle materials, Theor. Appl. Fract. Mech. 109 (2020).
[11] B.I.G. Barr, M.K. Lee, E.J. de Place Hansen, D. Dupont, E. Erdem, S. Schaerlaekens, B. Schnütgen, H. Stang, L. Vandewalle, Round-robin analysis of the RILEM TC 162-TDF beam-bending test: Part 1—Test method evaluation, Mater. Struct. 36(9) (2003) 609-620.
[12] A.N. Amirkhanian, D.W. Spring, J.R. Roesler, G.H. Paulino, Forward and Inverse Analysis of Concrete Fracture Using the Disk-Shaped Compact Tension Test, J. Test. Eval. 44(1) (2016).
[13] E. Brühwiler, F.H. Wittmann, The wedge splitting test, a new method of performing stable fracture mechanics tests, Eng. Fract. Mech. 35(1) (1990) 117-125.
[14] B.I.G. Barr, M.K. Lee, B. Barragán, D. Dupont, R. Gettu, J.F. Olesen, H. Stang, L. Vandewalle, Round-robin analysis of the RILEM TC 162-TDF uni-axial tensile test: Part 1, Mater. Struct. 36(4) (2003) 265-274.

[15] A. Carpinteri, S. Valente, G. Ferrara, G. Melchiorrl, Is mode II fracture energy a real material property?, Comput. Struct. 48(3) (1993) 397-413.
[16] G.A. Rao, B.K. Raghu Prasad, Influence of type of aggregate and surface roughness on the interface fracture properties, Mater. Struct. 37(5) (2004) 328-334.
[17] L. Hong, X. Gu, F. Lin, Influence of aggregate surface roughness on mechanical properties of interface and concrete, Constr. Build. Mater. 65 (2014) 338-349.
[18] X. Gu, L. Hong, Z. Wang, F. Lin, Experimental study and application of mechanical properties for the interface between cobblestone aggregate and mortar in concrete, Constr. Build. Mater. 46 (2013) 156-166.
[19] W. Dong, Z. Wu, X. Zhou, N. Wang, G. Kastiukas, An experimental study on crack propagation at rock-concrete interface using digital image correlation technique, Eng. Fract. Mech. 171 (2017) 50-63.
[20] Z. Yang, X. Frank Xu, A heterogeneous cohesive model for quasi-brittle materials considering spatially varying random fracture properties, Comput. Method. Appl. M. 197(45-48) (2008) 4027-4039.
[21] Z.J. Yang, X.T. Su, J.F. Chen, G.H. Liu, Monte Carlo simulation of complex cohesive fracture in random heterogeneous quasi-brittle materials, Int. J. Solids. Struct. 46(17) (2009) 3222-3234.
[22] X. Wang, Z. Yang, A.P. Jivkov, Monte Carlo simulations of mesoscale fracture of concrete with random aggregates and pores: a size effect study, Constr. Build. Mater. 80 (2015) 262-272.
[23] X.F. Wang, Z.J. Yang, J.R. Yates, A.P. Jivkov, C. Zhang, Monte Carlo simulations of mesoscale fracture modelling of concrete with random aggregates and pores, Constr. Build. Mater. 75 (2015) 35-45.
[24] W. Trawiński, J. Bobiński, J. Tejchman, Two-dimensional simulations of concrete fracture at aggregate level with cohesive elements based on X-ray μCT images, Eng. Fract. Mech. 168 (2016) 204-226.
[25] A. Tabiei, W. Zhang, Cohesive element approach for dynamic crack propagation: Artificial compliance and mesh dependency, Eng. Fract. Mech. 180 (2017) 23-42.
[26] W. Trawiński, J. Tejchman, J. Bobiński, A three-dimensional meso-scale modelling of concrete fracture, based on cohesive elements and X-ray μCT images, Eng. Fract. Mech. 189 (2018) 27-50.
[27] W. Ren, Z. Yang, R. Sharma, S.A. McDonald, P.M. Mummery, Three-Dimensional In Situ XCT Characterisation and FE Modelling of Cracking in Concrete, Complexity 2018 (2018) 1-11.
[28] L. Yang, Z.D. Li, Inverse Analysis of Rock Creep Model Parameters Based on Improved Simulated Annealing Differential Evolution Algorithm, Geotech. Geol. Eng. 37(2) (2019) 639-649.
[29] Y.P. Cao, N. Hu, Z.H. Yao, H. Fukunaga, An Inverse Approach for Constructing the Residual Stress Caused by Welding, in: M. Tanaka, G.S. Dulikravich (Eds.), Inverse Problems in Engineering Mechanics III, Elsevier Science Ltd, Oxford, 2002, pp. 201-208.
[30] B. Shen, G.H. Paulino, Identification of cohesive zone model and elastic parameters of fiber-reinforced cementitious composites using digital image correlation and a hybrid inverse technique, Cem. Concr. Compos. 33(5) (2011) 572-585.
[31] B.C. Hill, O. Giraldo-Londoño, G.H. Paulino, W.G. Buttlar, Inverse Estimation of Cohesive Fracture Properties of Asphalt Mixtures Using an Optimization Approach, Exp. Mech. 57(4) (2017) 637-648.
[32] S. Yang, X. Xi, K. Li, C.Q. Li, Numerical Modeling of Nonuniform Corrosion-Induced Concrete Crack Width, J. Struct. Eng. 144(8) (2018) 04018120.

[33] S.T. Yang, K.F. Li, C.Q. Li, Numerical determination of concrete crack width for corrosion-affected concrete structures, Comput. Struct. 207 (2018) 75-82.
[34] X. Xi, S. Yang, C.Q. Li, M. Cai, X. Hu, Z.K. Shipton, Meso-scale mixed-mode fracture modelling of reinforced concrete structures subjected to non-uniform corrosion, Eng. Fract. Mech. 199 (2018) 114-130.
[35] P. Grassl, M. Jirásek, Meso-scale approach to modelling the fracture process zone of concrete subjected to uniaxial tension, Int. J. Solids. Struct. 47(7-8) (2010) 957-968.
[36] B.S. Institution, Specification for Aggregates from Natural Sources for Concrete, London, 1992.
[37] A. 211.1-91, Standard Practice for Selecting Proportions for Normal, Heavyweight, and Mass Concrete, 2009.
[38] G.A. Rao, Generalization of Abrams' law for cement mortars, Cem. Concr. Res. 31(3) (2001) 495-502.
[39] R. S., N. P., Artificial Intelligence: A Modern Approach (3rd Edition), Prentice Hall2009.
[40] G. Papazafeiropoulos, M. Muñiz-Calvente, E. Martínez-Pañeda, Abaqus2Matlab: A suitable tool for finite element post-processing, Adv. Eng. Software 105 (2017) 9-16.
[41] W. Dong, D. Yang, X. Zhou, G. Kastiukas, B. Zhang, Experimental and numerical investigations on fracture process zone of rock-concrete interface, Fatig. Fract. Eng. Mater. Struct. 40(5) (2017) 820-835.
[42] P. Zhang, X. Hu, S. Yang, W. Yao, Modelling progressive failure in multi-phase materials using a phase field method, Eng. Fract. Mech. 209 (2019) 105-124.
[43] H. Gercek, Poisson's ratio values for rocks, Int. J. Rock Mech. Min. Sci. 44(1) (2007) 1-13.

565 **LIST OF TABLES**

569

570 Table 1 Mechanical parameters for different material phases of concrete

Description	Symbol	Values
Young's modulus of aggregate	E_{Agg}	80 GPa [24]
Young's modulus of mortar	E_{Mor}	23 GPa [24]
Poisson's ratio of aggregate	v_{Agg}	0.16 [43]
Poisson's ratio of mortar	v_{Mor}	0.22 [24]
Tensile strength of mortar	σ_{Mor}	2.2 MPa [16, 38]
Fracture energy of mortar	G_{Mor}	72 N/m [16, 38]
Failure displacement of mortar	$\delta_{\mathrm{f,Mor}}$	0.23 mm
Evolution rate parameter	α	7 [11]
Tensile strength of ITZ	σ_{ITZ}	0.55 MPa
Fracture energy of ITZ	G_{ITZ}	11 N/m
Failure displacement of ITZ	$\delta_{\mathrm{f,ITZ}}$	0.14 mm

571

572

573 Table 2 Optimized ITZ fracture properties for different heterogeneous models

Random heterogeneous model	Tensile strength (MPa)	Fracture energy (N/m)	Strength ratio of ITZ to mortar	Fracture energy ratio of ITZ to mortar	Error
1	1.02	28.9	0.46	0.40	1.8%
2	0.98	18.7	0.45	0.26	0.8%
3	0.96	17.1	0.44	0.24	2.9%
4	1.01	21.2	0.46	0.29	1.8%
5	1.01	15.9	0.46	0.22	3.1%
6	1.03	24.1	0.47	0.33	2.6%
7	1.01	26.3	0.46	0.37	1.2%
8	1.03	28.1	0.47	0.39	0.6%
9	0.96	13.1	0.44	0.18	0.7%
10	0.97	15.7	0.44	0.22	1.9%
Mean	1.00	20.9			
CoV	2.8%	27%			

574

575

576 Table 3 Optimized ITZ fracture properties for different values of mortar strength and fracture

577 energy

Mortar Strength	Mortar fracture energy	ITZ Tensile strength	ITZ fracture energy	Strength ratio of ITZ to mortar	Fracture energy ratio of ITZ to mortar	Error
1.9 MPa	72 N/m	1.11 MPa	31.9 N/m	0.58	0.44	1.3%
2.2 MPa	72 N/m	1.03 MPa	28.1 N/m	0.47	0.39	0.6%
2.5 MPa	72 N/m	0.94 MPa	22.5 N/m	0.38	0.31	0.6%
2.2 MPa	60 N/m	1.06 MPa	35.0 N/m	0.48	0.58	3.6%
2.2 MPa	94 N/m	1.13 MPa	30.3 N/m	0.51	0.32	0.6%

578

579

580

LIST OF FIGURES

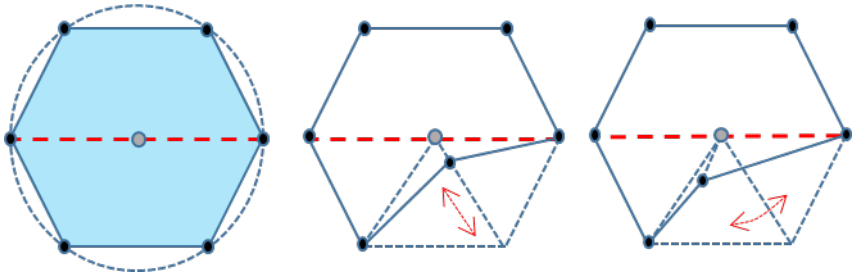

Figure 1 Generation of the irregular polygon: (a) regular polygon; (b) moving vertex; (c) rotating vertex

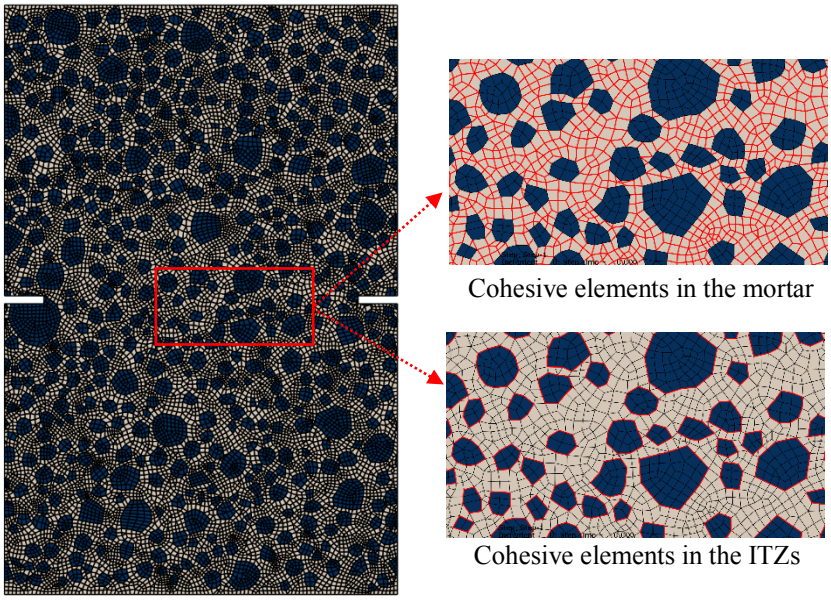

610

611 Figure 2 Meso-scale concrete model with cohesive elements

612

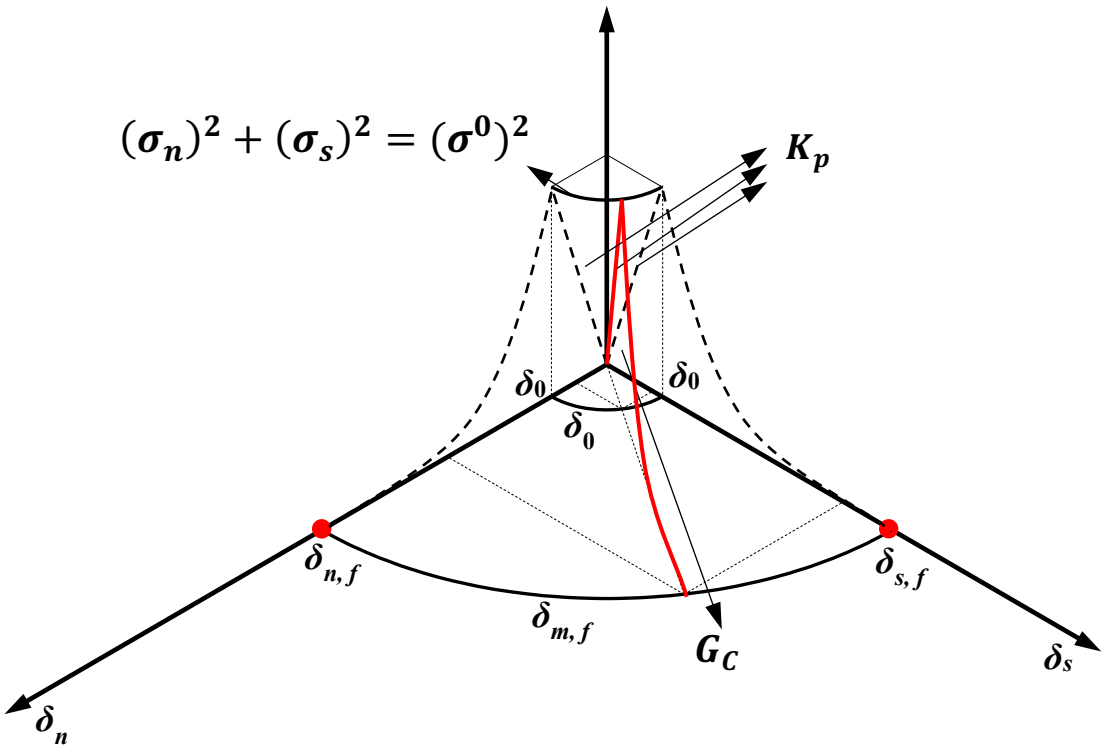

613

614 Figure 3 Stress-displacement relationship for the cohesive element

615

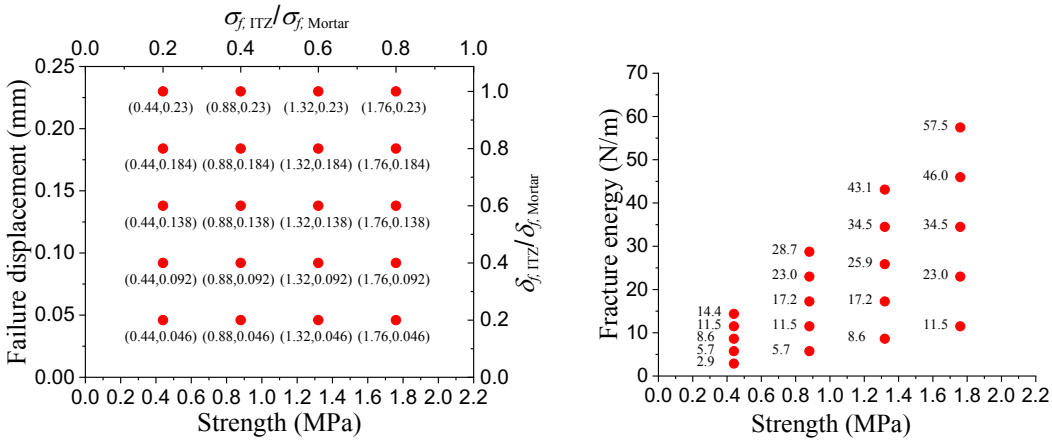

Figure 4 The initial values for ITZ fracture properties in the simulations for training (a) the strength and failure displacement; (b) the corresponding values of fracture energy

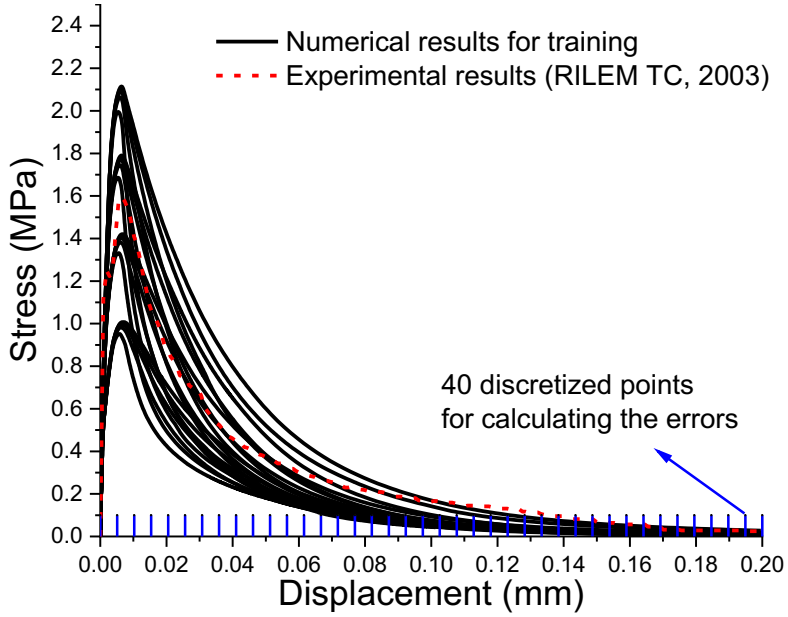

621

622 Figure 5 Stress-displacement curves for training neutral network

623

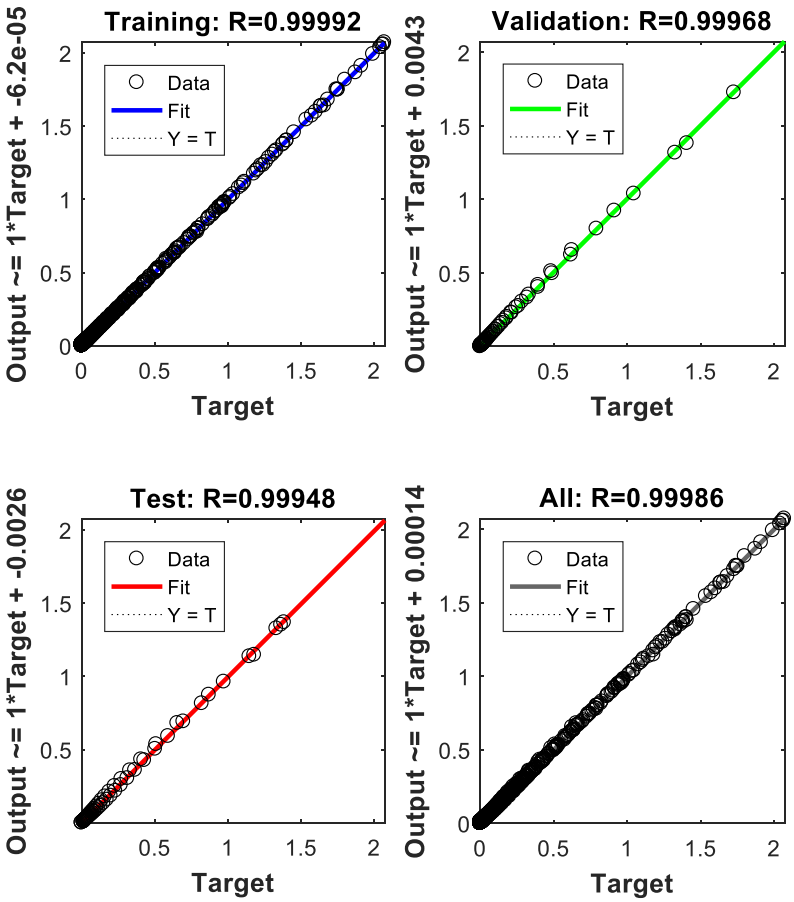

Figure 6 The regressions of network outputs with respect to targets for (a) training set; (b) validation set; (c) test set; (d) all data

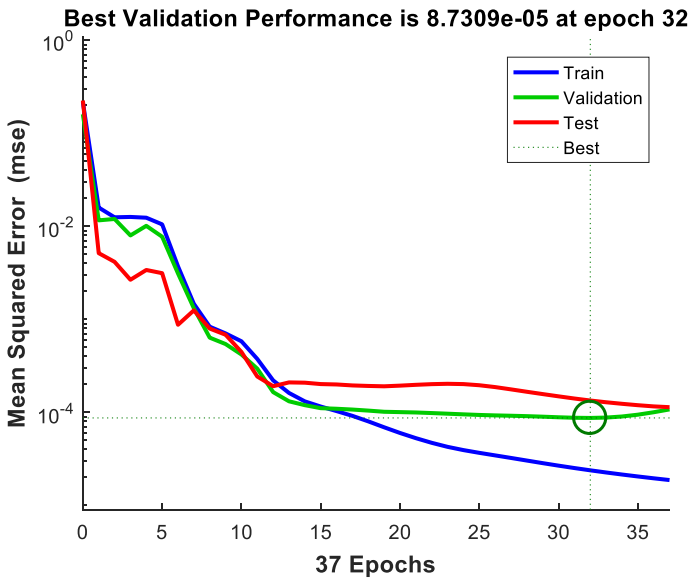

Figure 7 Mean squared errors of the network data with the epoch increasing

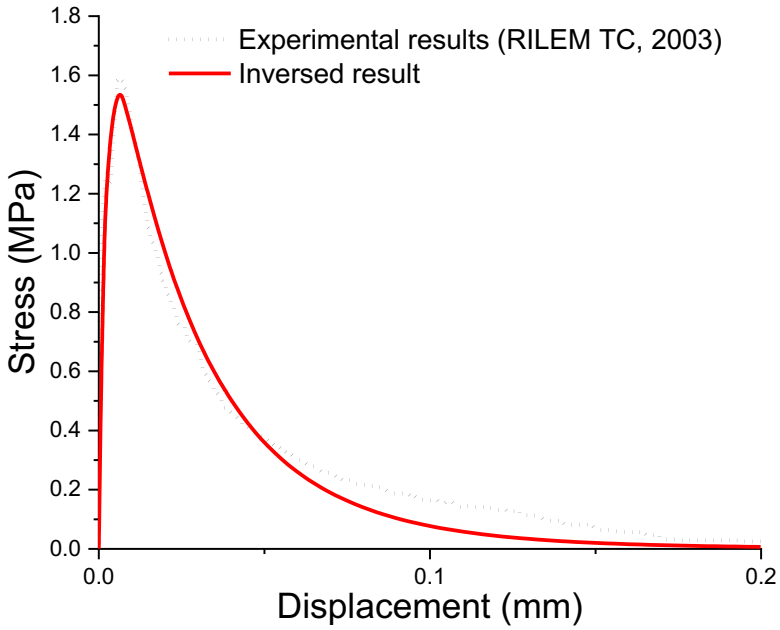

633

634 Figure 8 Stress-displacement curves from the experiment and numerical result with inversed
635 ITZ fracture properties

636

637

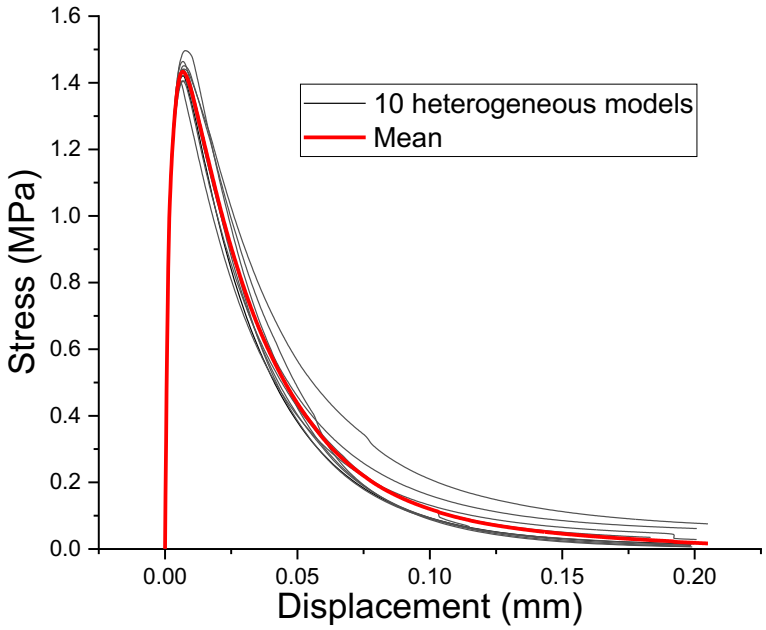

638

639 Figure 9 Effect of aggregate randomness on the stress-displacement curve

640

641

642

643

644

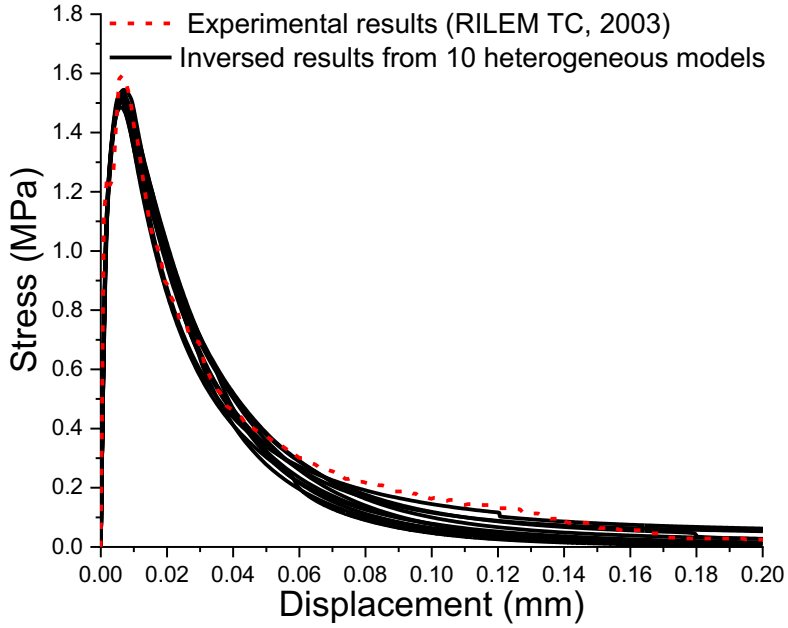

645

646 Figure 10 Stress-displacement curves from the experiment and inversed results for 10
647 heterogeneous models

648

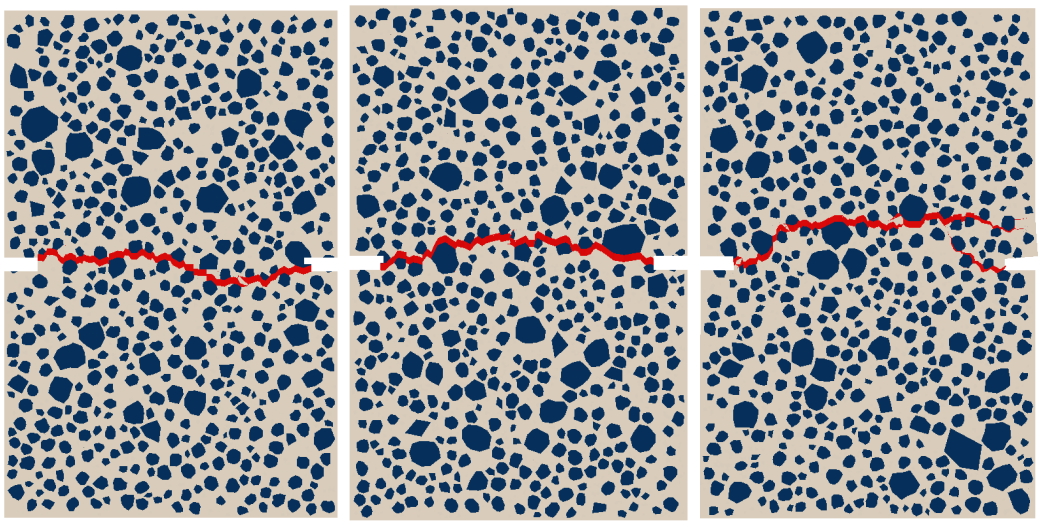

Figure 11 Typical crack patterns from the inversed results

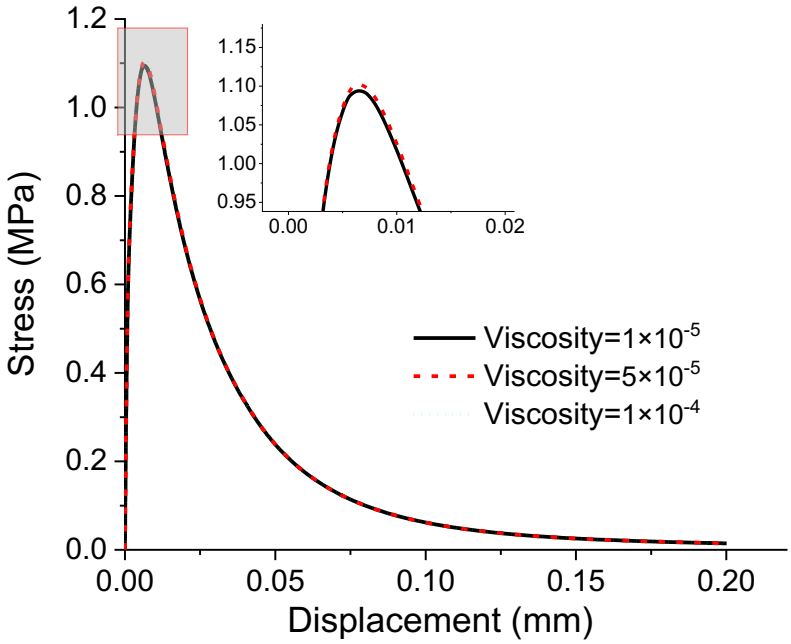

652

653 Figure 12 Effect of the viscosity on the stress-displacement curve of concrete

654

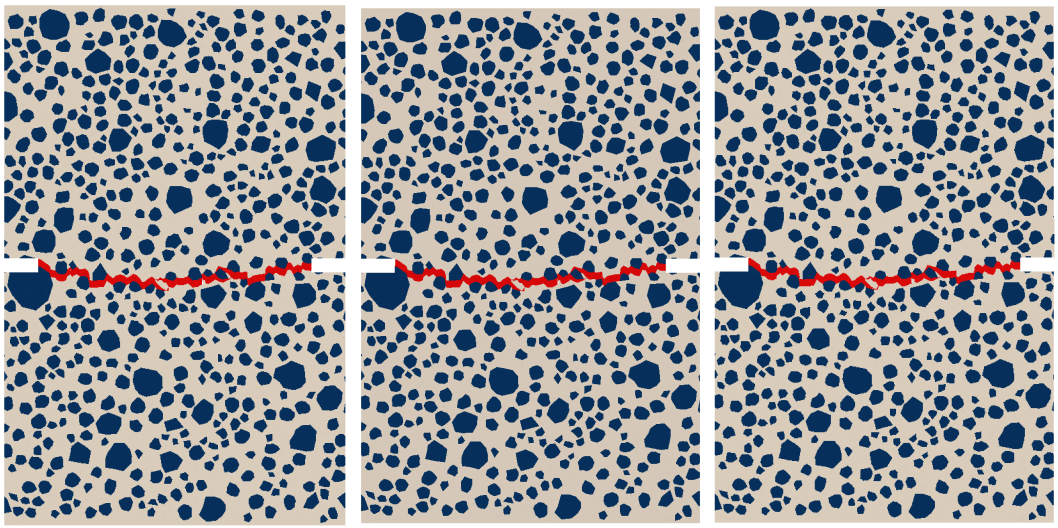

(a) viscosity=1.0×10^{-5} (b) viscosity=5.0×10^{-5} (c) viscosity=1.0×10^{-4}

Figure 13 Effect of the viscosity on the crack patterns of concrete

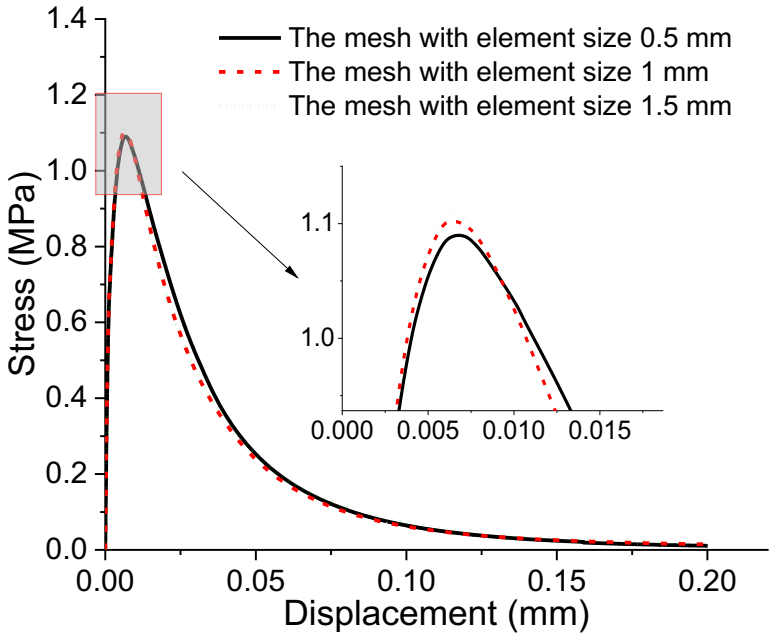

660

661 Figure 14 Effect of element size on the stress-displacement curve of concrete

662

663

664

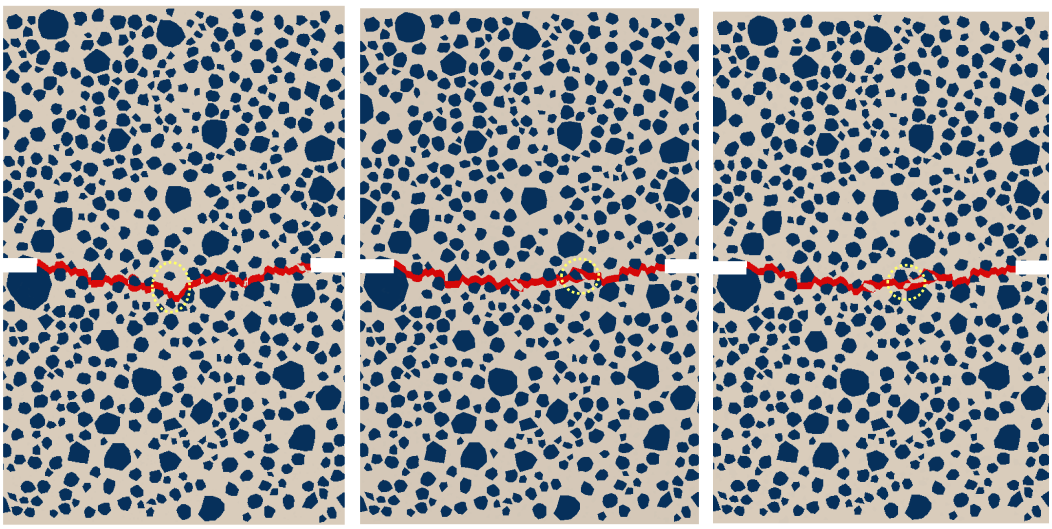

(a) element size 0.5 mm (b) element size 1 mm (c) element size 1.5 mm

Figure 15 Effect of element size on the crack patterns of concrete

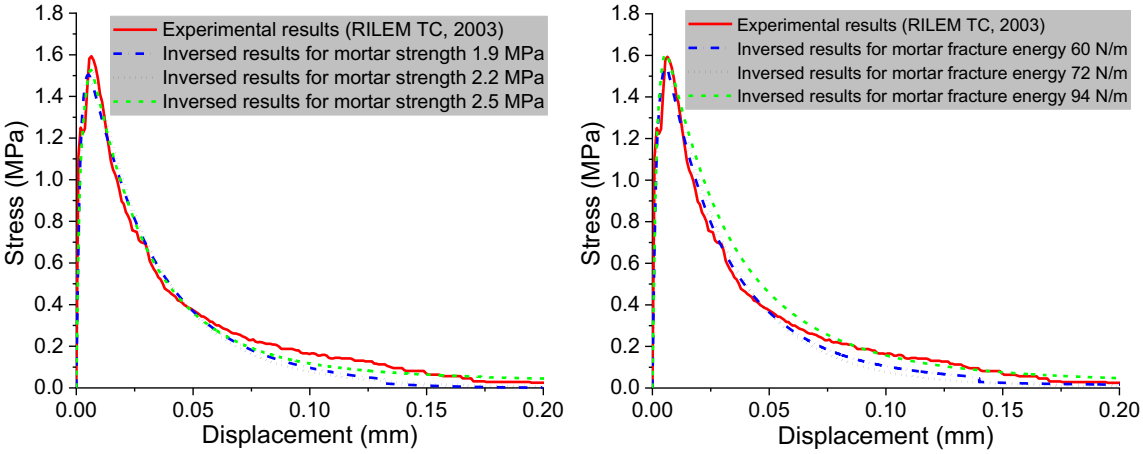

(a) Effect of mortar strength (b) Effect of mortar fracture energy

Figure 16 Stress-displacement curves from inversed results for different values of mortar fracture properties

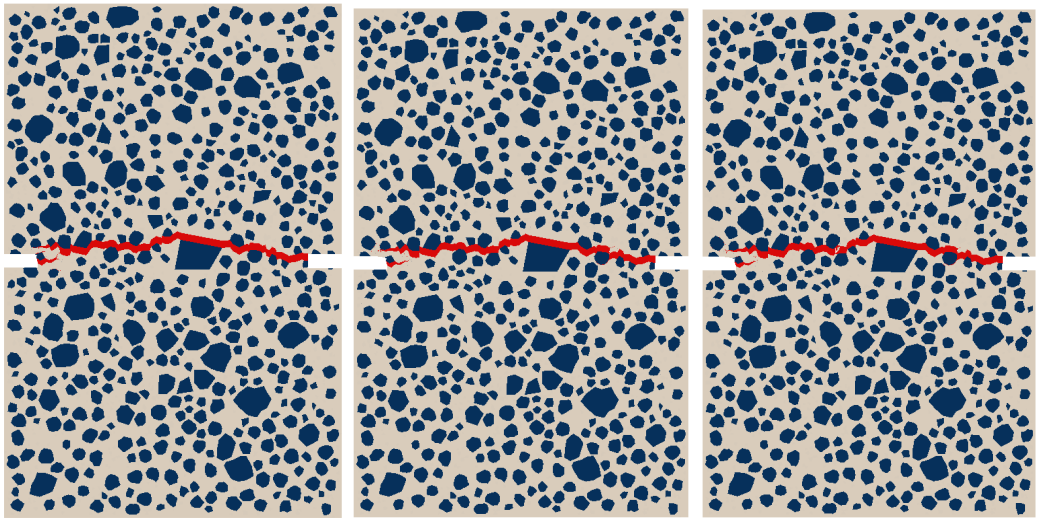

(a) σ_{Mor}=1.9 MPa, G_{Mor}=72 N/m (b) σ_{Mor} =2.2 MPa, G_{Mor}=72 N/m (c) σ_{Mor} =2.5 MPa, G_{Mor} =72 N/m

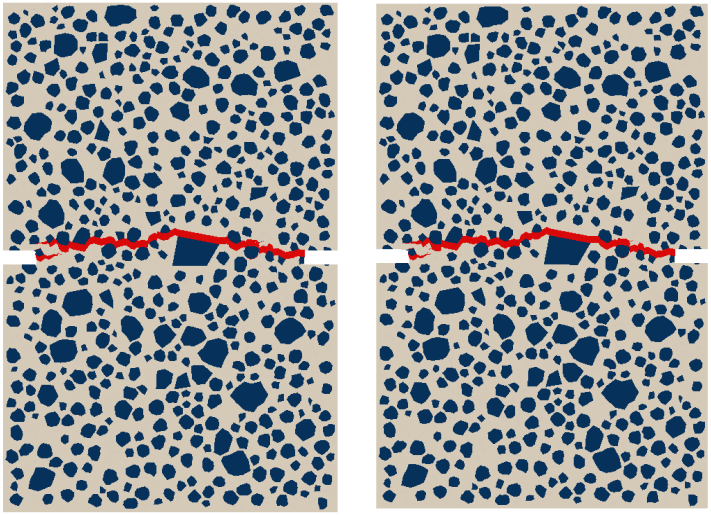

(d) σ_{Mor}=2.2 MPa, G_{Mor}=60 N/m (e) σ_{Mor}=2.2 MPa, G_{Mor}=94 N/m

Figure 17 Crack patterns of the inversed results for different values of mortar fracture properties